5200 *Biochemistry* **2010,** *49,* 5200–5205
DOI: 10.1021/bi100412v

BIOCHEMISTRY
including biophysical chemistry & molecular biology
Article

Structural Analysis of Botulinum Neurotoxin Type G Receptor Binding[†,‡]

John Schmitt,[§] Andrew Karalewitz,[@] Desirée A. Benefield,[§] Darren J. Mushrush,[∥] Rory N. Pruitt,[§] Benjamin W. Spiller,[⊥] Joseph T. Barbieri,*[,@] and D. Borden Lacy*[,§]

[§]*Department of Microbiology and Immunology,* [∥]*Department of Biochemistry, and* [⊥]*Department of Pharmacology, Vanderbilt University School of Medicine, Nashville, Tennessee 37232, and* [@]*Department of Microbiology and Molecular Genetics, Medical College of Wisconsin, Milwaukee, Wisconsin 53226*

Received March 17, 2010; Revised Manuscript Received May 20, 2010

ABSTRACT: Botulinum neurotoxin (BoNT) binds peripheral neurons at the neuromuscular junction through a dual-receptor mechanism that includes interactions with ganglioside and protein receptors. The receptor identities vary depending on BoNT serotype (A−G). BoNT/B and BoNT/G bind the luminal domains of synaptotagmin I and II, homologous synaptic vesicle proteins. We observe conditions under which BoNT/B binds both Syt isoforms, but BoNT/G binds only SytI. Both serotypes bind ganglioside G_{T1b}. The BoNT/G receptor-binding domain crystal structure provides a context for examining these binding interactions and a platform for understanding the physiological relevance of different Syt receptor isoforms in vivo.

Botulinum neurotoxin (BoNT)[1] is the causative agent of botulism, a potentially lethal neuroparalytic condition in humans (*1*). The extreme potency of BoNT ($LD_{50} \sim 0.1$ ng/kg) stems from the toxin's high affinity for neuronal receptors at the neuromuscular junction and enzymatic inhibition of neurotransmitter release (*2*). BoNTs are produced as single-chain proteins in seven antigenically distinct forms (serotypes A−G). Most BoNT serotypes undergo post-translational cleavage to form a dichain molecule composed of a light chain and a heavy chain linked by a disulfide bond. The light chain (LC) is a zinc metalloprotease that cleaves SNARE proteins to inhibit fusion of the neurotransmitter vesicle to the plasma membrane (*3*). The N-terminal half of the heavy chain (HCT) is involved in translocation of the LC across the endosomal membrane, and the C-terminal half of the heavy chain (HCR) is involved in binding receptors (*4*).

BoNT targets the neuromuscular junction through specific interactions with both ganglioside and protein receptors (*5*). BoNTs bind G_{D1a} and gangliosides in the G_{1b} series and show the highest affinity for the trisialoganglioside, G_{T1b} (*6*). The protein receptor can vary with BoNT serotype. Synaptotagmin I and II (SytI and SytII, respectively) mediate the internalization of BoNT/B and BoNT/G, but not BoNT/A or BoNT/E, into neuronal cells (*7*−*9*). SytI and SytII are homologous calcium sensors that couple neuronal calcium influx to the fast phase of neurotransmitter release (*10*). BoNT/B and BoNT/G bind to the luminal domains of SytI and SytII following the fusion of synaptic vesicles with the plasma membrane. The ability of a peptide, corresponding to 20 amino acids of the SytII luminal domain, in conjunction with gangliosides, to neutralize BoNT/B toxicity in mice is consistent with the SytII luminal domain being the neuronal receptor for BoNT/B (*7*).

BoNT/G is a recently discovered serotype whose HCR shares a high degree of primary amino acid conservation with BoNT/B (50% identical, 71% similar). Despite the homology between BoNT/B and BoNT/G and between SytI and SytII, several differences exist in their interactions with neurons. BoNT/B binds SytII in a manner independent of ganglioside but requires ganglioside to bind SytI (*7*). BoNT/G binds SytI and SytII in a ganglioside-independent manner (*8*). The ganglioside requirement is thought to reflect a situation in which the BoNT−protein receptor affinity is too weak to promote a stable, productive interaction. This hypothesis is supported by isothermal titration calorimetry showing that in the absence of ganglioside the affinity of BoNT/B for SytII is 34 nM, ∼100-fold greater than that for SytI. GST pull-down experiments showed that the BoNT/G HCR bound both SytI and SytII. This study did not report a preference for either Syt isoform in BoNT/G HCR binding or BoNT/G neutralization (*8*). In this study, we analyze the crystal structure of the BoNT/G HCR to improve our understanding of how BoNT/B and BoNT/G differ in their specificities for the two synaptotagmin isoforms and how they recognize their ganglioside coreceptor.

EXPERIMENTAL PROCEDURES

Generation of the BoNT/G HCR Expression Vector. A previously described BoNT/G HCR pET28a expression vector (*11*) was modified to delete a 3×FLAG sequence from the N-terminus. This change was made to remove unstructured regions of the protein but also resulted in a significant decrease in protein solubility. In an effort to improve solubility, residues 1080−1084 were mutated from the naturally occurring SSLYW BoNT/G sequence to the sequence observed in BoNT/B, EERYK. Mutations were made with the QuickChange protocol for site-directed mutagenesis and verified by sequencing.

Protein Expression and Purification. For the BoNT/G HCR, *Escherichia coli* BL21(DE3) cells harboring the BoNT/G

[†]J.T.B. acknowledges membership within and support from Region V 'Great Lakes RCE' (National Institutes of Health Grant 2-U54-AI-057153). D.B.L. was supported by National Institute of Allergy and Infectious Diseases Grant AI075259.

[‡]Coordinates and data have been deposited in the Protein Data Bank as entry 3MPP.

*To whom correspondence should be addressed. J.T.B.: e-mail, jtb01@mcw.edu; phone, (414) 456-8412. D.B.L.: e-mail, borden.lacy@vanderbilt.edu; phone, (615) 343-9080; fax, (615) 936-2211.

[1]Abbreviations: BoNT, botulinum neurotoxin; Syt, synaptotagmin; LC, light chain; HCT, heavy chain translocation domain; HCR, heavy chain receptor-binding domain; rmsd, root-mean-square deviation; PDB, Protein Data Bank.

 Published on Web 05/27/2010

HCR expression vector were grown in LB broth supplemented with 50 μg/mL kanamycin at 37 °C with shaking. At an OD_{600} of ~0.6, the temperature was reduced to 16 °C and 1 mM IPTG was added. Cells were harvested after 16−20 h by centrifugation and lysed with a French press. The protein was bound to His-Select nickel affinity gel (Sigma-Aldrich) and washed with buffers containing 50 mM KP_i (pH 8.5), 10 mM imidazole, and 500−700 mM NaCl. The BoNT/G HCR was eluted with a buffer containing 50 mM KP_i (pH 8.5), 50 mM NaCl, and 150 mM imidazole. The resulting eluate was applied to a GE Healthcare HiTrap Q HP ion exchange column. The flowthrough was incubated in 6 mM sodium iodoacetate for 30 min and immediately injected onto a GE Healthcare HiLoad 16/60 Superdex 200 size exclusion column using a buffer of 20 mM Tris (pH 7.5) and 100 mM KCl. For the BoNT/A and BoNT/B HCR, the construction of plasmids encoding the BoNT/A and BoNT/B HCR domains (pET-HCR/A and pET-HCR/B, respectively) with an N-terminal six-His and 3×FLAG sequence has been previously described (*11*). *E. coli* BL21(DE3) cells harboring these plasmids were grown in LB broth supplemented with 50 μg/mL kanamycin at 30 °C for 2 h with shaking. At an OD_{600} of ~0.6, the temperature was reduced to 16 °C and 0.1 mM IPTG was added. Cells were harvested after ~16 h by centrifugation and lysed with a French press. Proteins were purified using nickel affinity gel and eluted with buffer containing 0.25 M imidazole. Eluted proteins were subjected to S200HR gel filtration [Sephacryl, Sigma, 600 mL of resin equilibrated in 10 mM Tris-HCl (pH 7.9), 0.2 M NaCl, 0.5 mM EDTA, and 0.1% Triton X-100]. The peak fractions were pooled and concentrated using nickel affinity gel. Purified HCR/A and HCR/B were dialyzed into 10 mM Tris-HCl (pH 7.9), 0.2 M NaCl, and 40% glycerol for storage.

Synaptotagmin Binding Assay. Three peptides were synthesized with an N-terminal cysteine residue: SytI (cgegkedafsklkekfmnelhk), SytII (cgesqedmfaklkeklfneink), and a scrambled negative control (ckeankgdlkemseglkfehfk) (Biosyn). Peptides were diluted to 10 μg/mL in binding buffer [0.1 M sodium phosphate, 0.15 M sodium chloride, and 10 mM EDTA (pH 7.2)] and adsorbed to maleimide-activated 96-well plates (Pierce) overnight. Unreacted maleimide groups were quenched with a cysteine solution, and the wells were washed three times with wash buffer [0.1 M sodium phosphate, 0.15 M sodium chloride, and 0.05% Tween 20 (pH 7.2)]. BoNT HCR proteins were normalized for protein concentration, diluted to 25 μg/mL in wash buffer, and bound to wells for 2 h. Wells were washed and then incubated with 0.5 μM His-Probe (an NTA−HRP conjugate sold by Pierce). The presence of HRP was detected using the 1-Step Ultra TMB-ELISA substrate (Pierce). Each well was assayed five times and averaged, and the experiment was repeated numerous times with multiple concentrations of peptide bound and protein incubated.

Ganglioside Binding Assay. One hundred microliters of G_{T1b} (0.1 mg/mL) (Matreya, Pleasant Gap, PA) in methanol was added to a 96-well, nonbinding microtiter plate (Corning, Corning, NY) and allowed to dry overnight. The plate was washed three times with PBS and then blocked with 1% BSA in 50 mM $NaCO_3$ (pH 9.6) for 1 h at 4 °C. The plate was washed three times with PBS and then the indicated wild-type HCR−His-Probe conjugate (100 μL/well) with PBS and 1% BSA for 1 h at 4 °C. After being washed three times with PBS, the plate was developed at room temperature with TMB substrate (100 μL/well, Thermo Scientific) for 30 min, the reaction was stopped with 1 M H_2SO_4, and the absorbance was read at 450 nm. Data were measured in duplicate and averaged, and nonspecific binding in a well without G_{T1b} was subtracted. Data were analyzed using Excel (Microsoft, Seattle, WA), and ranges of the HCR yielding dose-dependent G_{T1b} binding were displayed using GraphPad Prism (GraphPad Software Inc., La Jolla, CA).

Table 1: X-ray Data Collection and Refinement Statistics[a]

Data Collection	
wavelength (Å)	0.9780
resolution (outer shell) (Å)	50−2.0 (2.03−2.0)
R_{merge}[b] (%)	10.4 (58.5)
mean $I/\sigma I$	16.8 (3.4)
completeness (%)	99.9 (100.0)
redundancy	4.2 (4.0)
no. of unique observations	33608 (1631)
Refinement	
R_{cryst}, R_{free}[c] (%)	17.47, 22.08
no. of protein atoms	3380
no. of ligand atoms	0
no. of solvent waters	348
bond length rmsd (Å)	0.007
bond angle rmsd (deg)	1.070
avg protein B (Å^2)	43.5
Ramachandran plot (%)	
most favored	319 (87.9%)
allowed	44 (12.1%)
generously allowed	0 (0.0%)
disallowed	0 (0.0%)

[a]Outer resolution bin statistics are given in parentheses. [b]$R_{merge} = \sum_{hkl}(\sum_i |I_{hkl,i} - \langle I_{hkl}\rangle|)/\sum_{hkl,i}\langle I_{hkl,i}\rangle$, where $I_{hkl,i}$ is the intensity of an individual measurement of the reflection with Miller indices h, k, and l and $\langle I_{hkl}\rangle$ is the mean intensity of that reflection. [c]$R_{cryst} = \sum||F_{obs,hkl}| - |F_{calc,hkl}||/|F_{obs,hkl}|$, where $|F_{obs,hkl}|$ and $|F_{calc,hkl}|$ are the observed and calculated structure factor amplitudes, respectively. R_{free} is equivalent to R_{cryst} but calculated with reflections (5%) omitted from the refinement process.

Crystallization. The purified BoNT/G HCR was concentrated to 11.5 ± 2 mg/mL and mixed 1:1 with mother liquor for hanging drop vapor diffusion crystallization. Reproducible crystals formed with mother liquor containing 12−15% (w/v) polyethylene glycol 3350, 20 mM Bis-Tris buffer (pH 5.75−6.50), and 20−25 mM MgCl. Crystals were preserved in a cryoprotectant of 15% ethylene glycol before being plunged into liquid nitrogen.

Structure Determination. X-ray data were obtained from a single crystal at 100 K on beamline 21-ID-G of the Advanced Photon Source. Diffraction data were indexed, integrated, scaled, and merged with HKL2000 (Table 1) (*12*). The crystal was in space group $P2_12_12_1$ and had unit cell dimensions of 57.63 Å (a), 90.16 Å (b), and 91.89 Å (c). Phases were determined by molecular replacement using the BoNT/B HCR structure (*13*) and MOLREP (*14*). The structure was subjected to iterative rounds of model building in Coot (*15*) and refinement in Phenix (*16*). Three TLS groups were assigned (1−213, 214−367, and 368−433) on the basis of tlsmd (*17*, *18*). The refined model (R_{cryst} = 17.47%, and R_{free} = 22.08%) consists of amino acids 867−920, 931−1036, 1039−1087, 1090−1157, 1165−1249, and 1259−1299 and 348 water molecules.

RESULTS AND DISCUSSION

Initial studies developed a direct binding assay for assessing interactions between the BoNT/G HCR and either Syt or ganglioside. Synthetic peptides corresponding to the luminal domains of SytI and SytII (or a scrambled negative control) were tethered

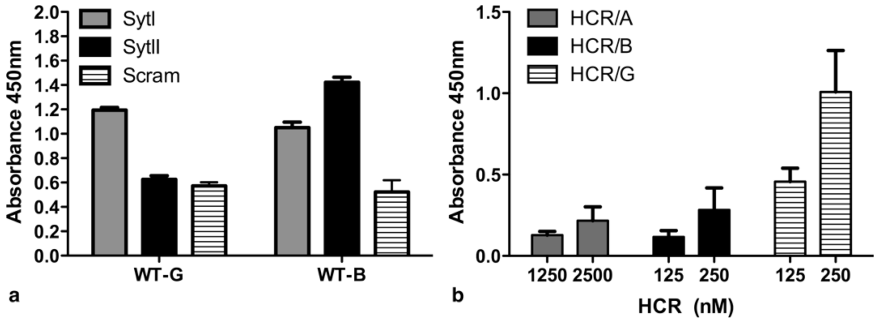

FIGURE 1: Direct assessment of BoNT/G binding to Syt and G_{T1b}. (a) Peptides from the luminal domains of SytI or SytII (or a scrambled negative control) were covalently linked to individual wells of maleimide-activated 96-well plates through N-terminal cysteine residues. Unbound peptide was washed away; unreacted maleimide groups were quenched, and wells were incubated with the excess BoNT/G and BoNT/B HCR (25 μg/mL) for 2 h at room temperature. Wells were washed five times and incubated with His-Probe (an NTA−horseradish peroxidase fusion). Addition of a TMB-ELISA substrate allowed colorimetric detection of bound protein. The average (with standard deviation) for five replicates is shown. (b) Nonbinding ELISA plates were coated with 10 μg of G_{T1b} per well in methanol and dried overnight. Plates were blocked in carbonate buffer, washed three times with PBS, and incubated with the indicated HCR−His-Probe conjugate for 1 h at 4 °C. The plate was washed and developed with TMB substrate for 30 min; the reaction was stopped with 1 M H_2SO_4, and the absorbance was read at 450 nm. Duplicate wells were averaged and subtracted from the absorbance detected in an uncoated well. Data are the average of two independent experiments. In both experiments, the mutated form of BoNT/G containing the EERYK solubility sequence was used. The six-His sequences are located at the N-terminus of the HCR domains and are not expected to interfere with Syt or ganglioside binding.

to a maleimide-activated solid support through an N-terminal cysteine residue. The BoNT/G or BoNT/B HCR was added in excess, and the relative amount of the bound HCR was determined. Syt peptide interactions were assessed in the absence of ganglioside. This analysis showed that while the BoNT/B HCR bound both isoforms of Syt, the BoNT/G HCR bound only the SytI peptide (Figure 1a).

The fact that BoNT/B showed a stronger interaction with SytII over SytI is consistent with previous reports (*7*−*9*). The fact that gangliosides were not required in either interaction could reflect an enhanced sensitivity for the ELISA-based method. We were surprised, however, to see that in our assay, BoNT/G interacted with only SytI. Previous binding interaction studies have been assessed with a GST pull-down assay in which GST−Syt fusion proteins are displayed on a glutathione Sepharose bead support. Bound proteins are eluted from the beads and subjected to SDS−PAGE (*7*−*9*). We assume that if the ELISA-based method were in fact more sensitive, we would have detected BoNT/G binding to both isoforms of Syt. Since the conditions for binding, washing, and detection differ significantly between the two assays, we are left with the conclusion that the mode in which BoNT/B and BoNT/G recognize SytI and SytII likely differs.

The capacity for the BoNT/G HCR to interact with gangliosides (G_{T1b}) was also determined (Figure 1b). BoNT/B and BoNT/G HCRs exhibited a similar, measurable association, which was stronger than the interaction of the BoNT/A HCR with G_{T1b}. This was somewhat unexpected, since the BoNT/A HCR is the only serotype that has been cocrystallized in the presence of a G_{T1b} headgroup (*19*). This suggested that HCR/B and HCR/G bound G_{T1b} with a higher affinity than HCR/A and motivated our investigation into the structural basis for how BoNT/G interacts with ganglioside.

Thus, the next goal was to obtain a structural context for understanding the Syt and ganglioside binding properties of the BoNT/G HCR. However, initial structural studies of the BoNT/G HCR were hampered by protein insolubility. In an effort to increase solubility, residues 1080−1084 of the BoNT/G HCR were mutated from SSLYW to EERYK. Residues 1080−1084 are located in the α-helix connecting the N-terminal β-barrel domain and C-terminal β-trefoil domain and therefore were not expected to affect the receptor binding sites that are

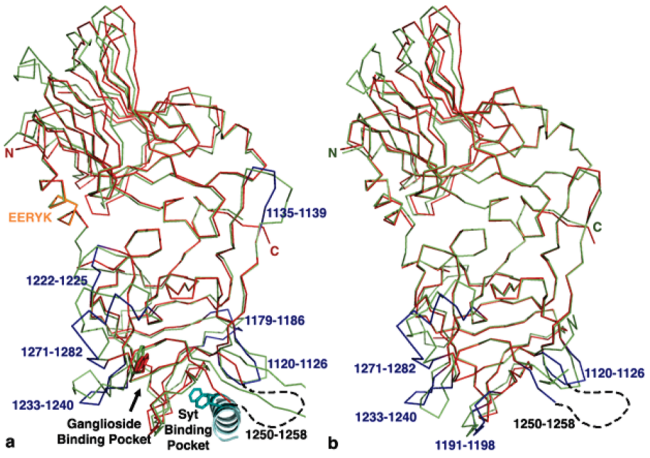

FIGURE 2: Comparison of BoNT/B and BoNT/G HCR structures. (a) The structure of the BoNT/G HCR (red) was aligned with the BoNT/B HCR (PDB entry 1EPW; green), and significant loop differences in BoNT/G are colored blue. The helix linking the N- and C-terminal subdomains (orange) was mutated to EERYK to improve solubility. The position of the SytII helix (teal) was identified in the BoNT/B HCR−SytII crystal structure (PDB entry 2NM1). Two SytII phenylalanine residues (F47 and F54; shown as sticks) dominate the interaction with BoNT/B. A conserved tryptophan residue (shown as sticks) is known to be important for ganglioside binding. (b) The structure of the BoNT/G HCR (red and blue, this study) was aligned with that of a different crystal form (PDB entry 2VXR; green). Significant loop differences in the C-terminal subdomain are colored blue.

located at the C-terminal region of the HCR. This substitution enhanced the solubility of the BoNT/G HCR and allowed conditions that produced a crystal that diffracted to 2.0 Å to be established (Table 1 and Figure 2). The BoNT/G HCR structure aligns with the structure of the BoNT/B HCR with an rmsd of 0.64 Å. The principle differences are located in surface loops of the β-trefoil domain and are highlighted in Figure 2a. Coincident with the efforts in our laboratory, another group determined a structure of the BoNT/G HCR using a different crystal form (*20*). The structures align with an rmsd of 0.44 Å and differ in the positions of some surface loops (Figure 2b).

Alignments were made between the Syt binding sites of BoNT/B and BoNT/G. Previous structures of BoNT/B bound to a SytII

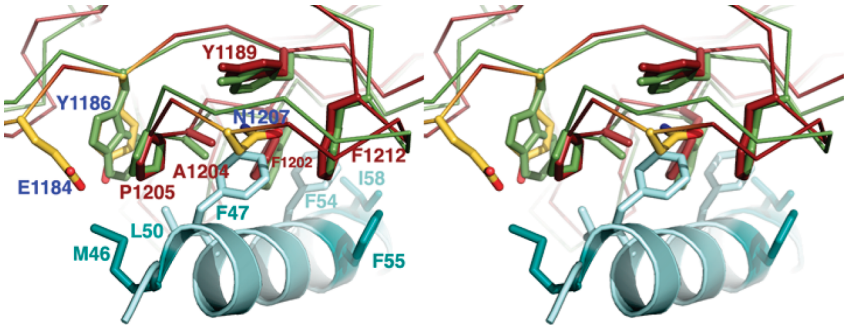

FIGURE 3: Structural conservation in the Syt binding site. A cross-eye stereo close-up of the F47 binding pocket indicates that five of the 12 residues making contact between BoNT/B and SytII are conserved in both identity and position in the structure of BoNT/G (red or green sticks to represent BoNT/G or BoNT/B, respectively). A sixth contact residue (BoNT/B W1178) is replaced by Y1186 in the BoNT/G structure. BoNT/G residues E1184 and N1207 (colored by atom) do not align with BoNT/B contact residues but are positioned so that they could have an impact on Syt binding. The coordinates for BoNT/B were taken from PDB entry 1EPW, while the SytII peptide (teal) is taken from the aligned PDB entry 2NM1. Residues that differ between SytI and SytII are colored dark teal, while conserved BoNT/B contact residues are colored light teal.

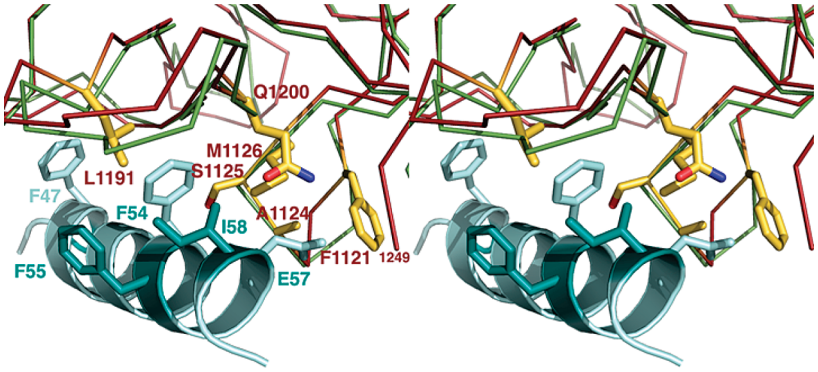

FIGURE 4: Structural divergence in the Syt binding site. A cross-eye stereo close-up of the F54 binding pocket indicates that the remaining six BoNT/B contact residues differ in BoNT/G. (Only the BoNT/G side chains are shown for the sake of clarity.) Four of the residues that differ (F1121, A1124, S1125, and M1126) are located on a loop whose backbone is positioned differently with respect to the corresponding loop of BoNT/B. The structure from this study is colored red, while BoNT/B (PDB entry 1EPW) is colored green. The SytII peptide (teal) is taken from the aligned PDB entry 2NM1. Residues that differ between SytI and SytII are colored dark teal, while conserved BoNT/B contact residues are colored light teal.

peptide have revealed a two-pocket binding site on BoNT/B (*21*, *22*). The pockets are defined by their interactions with one of two phenylalanine residues, F47 or F54, which are present in many SytI and SytII sequences. In BoNT/B, the pockets are lined by 12 amino acids, five of which are conserved in BoNT/G. In the BoNT/G structure, the five conserved amino acids (Y1189, F1202, A1204, P1205, and F1212) align closely with the position of the corresponding BoNT/B residues and line the F47 pocket (Figure 3). BoNT/B W1178, which is known to contact M46 of SytII, is changed to Y1186 in BoNT/G, which could be relevant for Syt specificity since in SytI, position 46 is an Ala residue. This change to a smaller residue might better accommodate the charge of BoNT/G E1184 as well. For either isoform, binding will require rearrangement of BoNT/G residue N1207, which is currently poised to clash with F47.

Unlike the F47 pocket, where several surface residues are conserved, more differences were observed between the BoNT/B and BoNT/G residues lining the F54 pocket. In this pocket, none of the six BoNT/B residues that interacted with SytII were conserved in BoNT/G (Figure 4). Three of these residues (M1126, L1191, and Q1200) have already been tested in a detailed mutagenesis study (*9*). The individual mutation of each residue (M1126D, L1191R, Q1200E, Q1200K, and Q1200Y) resulted in a significant loss of binding to SytI and SytII in a GST pull-down assay and a detectable loss of toxicity in a mouse phrenic nerve assay. The most significant toxicity defect was observed for Q1200K, a mutation to the corresponding residue in BoNT/B. This led the authors to conclude that Q1200 is central to the specificity differences between BoNT/B and BoNT/G (*9*).

The three contact residues that were not mutated in the previous study (F1121, A1124, and S1125) are located along with M1126 in the sequence of residues 1120−1126 (YFSKASM) of BoNT/G (Figure 4). We propose that differences in both the side chain and backbone positions of this loop could impact the specificity and affinity for Syt receptors. Another loop that might be located in the vicinity of the F54 pocket was loop 1250−1258; however, this loop was not observed in our electron density maps of the BoNT/G HCR (Figure 2a) and was only partially visible and oriented differently in the other crystal form (Figure 2b) (*20*). In the BoNT/B−SytII structure, contacts were not observed between SytII and corresponding loop 1244−1253 of BoNT/B. Finally, we note that the side chain positions of many of the residues in the F54 pocket (F1121, M1126, L1191, Q1200, and F1202) differ between the two BoNT/G HCR structures. This is the likely result of differences in crystal contacts, present here in both crystal forms, and illustrates the fact that this region is capable of reorganization with a potential for multiple binding modes depending on the nature of the available ligand.

In summary, while BoNT/B is capable of binding both SytI and SytII, our assay of SytI−SytII binding indicates that the BoNT/G HCR specifically binds SytI. Analysis of the BoNT/B and BoNT/G Syt binding sites suggests that specificity differences are likely to stem from differences in the "F54 subsite".

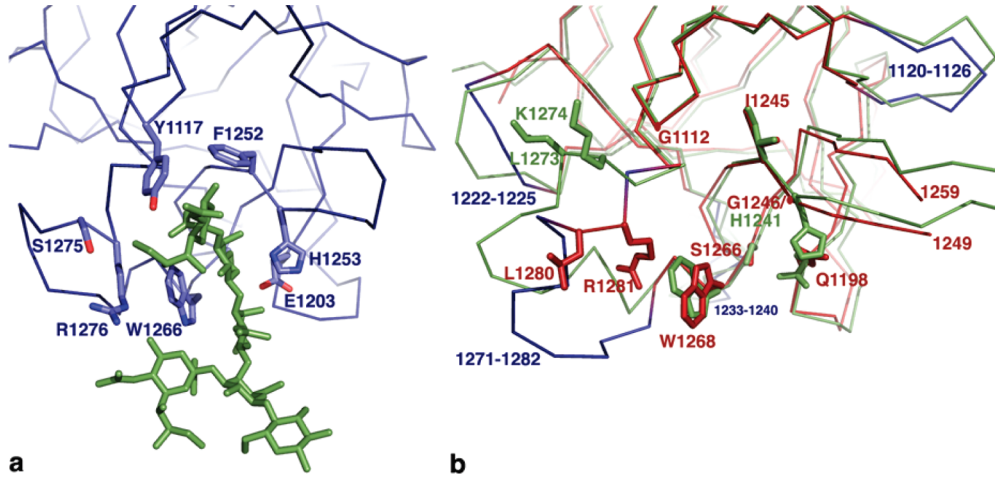

FIGURE 5: Ganglioside binding site. (a) The structure of BoNT/A bound to G_{T1b} reveals eight residues (depicted as sticks) that had contact with the G_{T1b} carbohydrate headgroup (green). (b) The corresponding residues in BoNT/G and BoNT/B are colored red and green, respectively. Most notably, BoNT/G has a glycine (G1246) in a position where BoNT/A, BoNT/B, and TeNT have a histidine. BoNT/G loops that differ significantly from the corresponding BoNT/B loops are colored blue. The altered position of loop 1271−1282 (blue) more closely resembles that observed in the BoNT/A−G_{T1b} structure and allows Arg1281 to buttress the tryptophan of the ganglioside binding site.

In addition to a number of amino acid differences that have been noted in point mutagenesis studies, we note a significant difference in the position of BoNT/G loop 1120−1126 relative to the position of the corresponding loop in BoNT/B. We also note that a crystal structure of BoNT/G from another crystal form has a number of structural differences due to crystal contacts. This observation suggests that the region is malleable and can change its structure in response to the properties of its ligand. In light of these data, we suggest that future efforts in deciphering the molecular basis of specificity differences consider the impact of entire loop substitutions in addition to that of single-point mutants.

Our assay of ganglioside binding indicates that the interaction of G_{T1b} with BoNT/A is measurable, but of lower affinity than that seen with BoNT/B and BoNT/G. There are a number of structural differences in the G_{T1b} binding site that could account for this difference in affinity. A crystal structure of BoNT/A bound to G_{T1b} revealed eight amino acids involved in direct contacts with the carbohydrate headgroup (Figure 5a). Only three of these residues are conserved in BoNT/G. Interestingly, two of these residues (W1268 and R1281) in BoNT/G are in different conformations versus what has been observed in other structures (Figure 5b). This could be the result of a crystallization contact that likely impacts the position of the R1271−R1281 loop. The altered position of loop 1271−1282 causes R1281 to be located within the ganglioside binding pocket. This position is different from the other BoNT/G HCR crystal form but is notable in its aligned proximity to BoNT/A R1276, a key residue in the interaction of BoNT/A with ganglioside (Figure 5a). In the other crystal form of the BoNT/G HCR, this position is occupied by R1272, suggesting the importance of arginine in supporting the key tryptophan of the ganglioside binding site. We propose that rearrangements in loop 1271−1282 of BoNT/G could allow the toxin to recognize different ganglioside headgroups. The structures of BoNT/B and BoNT/G have more space at the top of the ganglioside binding site due to the substitution of BoNT/A residues Y1117 and F1252 with glycine and isoleucine, respectively. Finally, we note that BoNT/G has a Gly1246 residue located at the base of the carbohydrate binding pocket, while most BoNT serotypes encode a histidine residue at this position (Figure 5b).

Our data suggest that BoNT/G binds G_{T1b} with an affinity higher than what has been observed for BoNT/A and that SytI and SytII be considered, not as homologues, but as distinct modes of entry for the BoNT/B and BoNT/G serotypes. A molecular understanding of the host−toxin interaction for botulism will require a detailed knowledge of which receptors are selected preferentially for entry in vivo. Efforts to dissect these in vivo entry mechanisms on the basis of structure-guided mutagenesis are underway.

REFERENCES

1. Simpson, L. L. (1981) The origin, structure, and pharmacological activity of botulinum toxin. *Pharmacol. Rev. 33*, 155–188.
2. Gill, D. M. (1982) Bacterial toxins: A table of lethal amounts. *Microbiol. Rev. 46*, 86–94.
3. Brunger, A. T., Jin, R., and Breidenbach, M. A. (2008) Highly specific interactions between botulinum neurotoxins and synaptic vesicle proteins. *Cell. Mol. Life Sci. 65*, 2296–2306.
4. Montecucco, C., Papini, E., and Schiavo, G. (1994) Bacterial protein toxins penetrate cells via a four-step mechanism. *FEBS Lett. 346*, 92–98.
5. Montecucco, C. (1986) How do tetanus and botulinum neurotoxins bind to neuronal membranes? *Trends Biochem. Sci. 11*, 314–317.
6. Kitamura, M., Iwamori, M., and Nagai, Y. (1980) Interaction between *Clostridium botulinum* neurotoxin and gangliosides. *Biochim. Biophys. Acta 628*, 328–335.
7. Dong, M., Richards, D. A., Goodnough, M. C., Tepp, W. H., Johnson, E. A., and Chapman, E. R. (2003) Synaptotagmins I and II mediate entry of botulinum neurotoxin B into cells. *J. Cell Biol. 162*, 1293–1303.
8. Rummel, A., Karnath, T., Henke, T., Bigalke, H., and Binz, T. (2004) Synaptotagmins I and II act as nerve cell receptors for botulinum neurotoxin G. *J. Biol. Chem. 279*, 30865–30870.
9. Rummel, A., Eichner, T., Weil, T., Karnath, T., Gutcaits, A., Mahrhold, S., Sandhoff, K., Proia, R. L., Acharya, K. R., Bigalke, H., and Binz, T. (2007) Identification of the protein receptor binding site of botulinum neurotoxins B and G proves the double-receptor concept. *Proc. Natl. Acad. Sci. U.S.A. 104*, 359–364.
10. Sudhof, T. C. (2004) The synaptic vesicle cycle. *Annu. Rev. Neurosci. 27*, 509–547.
11. Baldwin, M. R., Tepp, W. H., Przedpelski, A., Pier, C. L., Bradshaw, M., Johnson, E. A., and Barbieri, J. T. (2008) Subunit vaccine against the seven serotypes of botulism. *Infect. Immun. 76*, 1314–1318.
12. Otwinowski, Z., and Minor, W. (1997) Processing of X-ray diffraction data collected in oscillation mode. *Macromol. Crystallogr. 276* (Part A), 307–326.
13. Swaminathan, S., and Eswaramoorthy, S. (2000) Structural analysis of the catalytic and binding sites of *Clostridium botulinum* neurotoxin B. *Nat. Struct. Biol. 7*, 693–699.

14. Vagin, A., and Teplyakov, A. (1997) MOLREP: An automated program for molecular replacement. *J. Appl. Crystallogr. 30*, 1022–1025.
15. Emsley, P., and Cowtan, K. (2004) Coot: Model-building tools for molecular graphics. *Acta Crystallogr. D60*, 2126–2132.
16. Adams, P. D., Grosse-Kunstleve, R. W., Hung, L. W., Ioerger, T. R., McCoy, A. J., Moriarty, N. W., Read, R. J., Sacchettini, J. C., Sauter, N. K., and Terwilliger, T. C. (2002) PHENIX: Building new software for automated crystallographic structure determination. *Acta Crystallogr. D58*, 1948–1954.
17. Painter, J., and Merritt, E. A. (2006) Optimal description of a protein structure in terms of multiple groups undergoing TLS motion. *Acta Crystallogr. D62*, 439–450.
18. Painter, J., and Merritt, E. A. (2005) A molecular viewer for the analysis of TLS rigid-body motion in macromolecules. *Acta Crystallogr. D61*, 465–471.
19. Stenmark, P., Dupuy, J., Imamura, A., Kiso, M., and Stevens, R. C. (2008) Crystal structure of botulinum neurotoxin type A in complex with the cell surface co-receptor GT1b-insight into the toxin-neuron interaction. *PLoS Pathog. 4*, e1000129.
20. Stenmark, P., Dong, M., Dupuy, J., Chapman, E. R., and Stevens, R. C. (2010) Crystal structure of the botulinum neurotoxin type G binding domain: Insight into cell surface binding. *J. Mol. Biol. 397*, 1287–1297.
21. Jin, R., Rummel, A., Binz, T., and Brunger, A. T. (2006) Botulinum neurotoxin B recognizes its protein receptor with high affinity and specificity. *Nature 444*, 1092–1095.
22. Chai, Q., Arndt, J. W., Dong, M., Tepp, W. H., Johnson, E. A., Chapman, E. R., and Stevens, R. C. (2006) Structural basis of cell surface receptor recognition by botulinum neurotoxin B. *Nature 444*, 1096–1100.